 FDMP, vol.7, no.1, pp.71-95, 2011

Combined Thermal Radiation and Laminar Mixed Convection in a Square Open Enclosure with Inlet and Outlet Ports

Mohamed Ammar Abbassi[1,2], **Kamel Halouani**[1], **Xavier Chesneau**[3]
Belkacem Zeghmati[3]

Abstract: Mixed convection inside a square cavity with inlet and outlet ports is numerically simulated considering thermal radiation effect. The non dimensional transfer equations, based on Boussinesq assumption and the radiative heat transfer equation are solved by the finite-volume-method and the TDMA algorithm. Results, presented for a gray fluid and a wide range of dimensionless numbers; Reynolds (Re=10-1000), Richardson (Ri=0-0.01), Boltzmann (Bo=0.1-100), radiation to conduction parameter (Rc=0.1-100), and optical thickness (τ =0.1-10) show that the radiation significantly affects temperature distribution. Streamlines are also sensitive to radiative parameters (as optical thickness) but less than temperature.

Keywords: combined, radiation, mixed convection, open cavity, optical thickness

Nomenclature

Bo	Boltzmann number, $Bo = \rho C_p U_e / n^2 \tilde{\sigma} T_h^3$
G	incident radiation, $G = \int_{\Omega=4\pi} I d\Omega$
Gr	Grashof number, $Gr = g\beta\Delta T d_e^3 / \nu^2$
I	radiation intensity, W m^{-2} Sr^{-1}
k	thermal conductivity, W m^{-1} K^{-1}
L	enclosure height, m
n	refractive index
Nu	Nusselt number
N	normalized direction cosine

[1] METS-IESG-ENIS, IPEIS, University of Sfax, B.P:1172 – 3018 – Sfax – Tunisie
[2] Corresponding author, Fax : +216 74 246 347; Email: MedAmmar.Abbassi@enim.rnu.tn
[3] LAMPS-GME, University of Perpignan Via Domitia, 52 Avenue Paul Alduy, 66860 Perpignan Cedex France

$\vec{n}$	unit normal vector
P	pressure, N m^{-2}
Pr	Prandtl number, Pr $= \nu/\alpha$
Rc	radiation to conduction parameter, $R_C = d_e n^2 \tilde{\sigma} T_h^3/k$
Re	Reynolds number, $Re = U_e d_e/\nu$
Ri	Richardson number, $Ri = Gr/Re^2$
r	reflectivity
T	temperature, K
t	time, s
u, v	velocity components in x and y directions respectively, m
x, y	rectangular coordinate, m

Greek symbols

α	thermal diffusivity, m^{2}s^{-1}
β	coefficient of thermal expansion, K^{-1}
κ_a	absorption coefficient, m^{-1}
θ	dimensionless temperature
μ, η	direction cosines
ν	kinematic viscosity, m^2 s^{-1}
ρ	density, kg m^{-3}
σ	scattering coefficient, m^{-1}
$\tilde{\sigma}$	Stefan-Boltzmann constant, 5.67×10^{-8}Wm^{-2}K^{-4}
Φ	scattering phase function
τ	optical thickness
Ψ	stream function, m^2 s^{-1}
ω	single scattering albedo
ε	wall emissivity
θ	dimensionless temperature
Ω	solid angle, sr

Subscripts

h	hot
c	cold
b	bulk, black body
e	inlet

s outlet

Superscripts

l, l' inward and outward directions

1 Introduction

The knowledge of flow structure and heat transfer by mixed convection inside open cavities is of interest in relation to numbers of engineering applications such as cooling of electronic components, finned heat exchangers, ventilation, evaporative cooling, fire control in buildings and combustion rooms. Buoyancy forces may aid or oppose the forced flow depending on their relative directions to the direction of inertia-driven flow causing an increase or decrease in heat transfer rates. Accary, Meradji, Morvan, and Fougere (2008) studied mixed convection in a rectangular channel heated from below in the case of large temperature variations. The Navier-Stokes equations, obtained under the assumption of a low Mach number flow, were solved using a finite volume method. The results, corresponding to the steady-state case of the benchmark, led to the idea of launching a call for contribution in order to set up a reference solution essential for the validation of future numerical codes. Omri and Ben Nasrallah (1999) studied mixed convection in a rectangular enclosure with differentially heated vertical side walls having openings for inlet and outlet. Two different placement configurations of the inlet and outlet openings on the side walls were investigated. In the first case, the cold air was injected at the top of the hot wall and exited at the bottom of the cold wall, whereas in the second configuration the air injection was at the lower edge of the hot wall and the exit at the top of the cold wall. A control-volume-finite-element method (CVFEM) using triangular elements is employed to discretize the governing equations. Improvement in cooling efficiency was found with the inlet placed at the bottom of the hot wall. Ben-Arous and Busedram (2008) investigated numerically combined free and forced convection in horizontal semicircular ducts with radial internal fins. The wall of the duct was assumed to have a uniform heat input along the axial direction with a uniform peripheral wall temperature. The governing equations were solved by using a control-volume-based finite-difference approach. The fluid flow and heat transfer characteristics were found to be dependent on the Grashof number, the fin length and the number of fins. The most remarkable outcome of the such study is that, for each number of fins an optimum fin length exists at which the Nusselt number is maximal. Papanicolaou and Jaluria (1990) studied numerically the mixed convection transport induced by an isolated heat source providing a uniform heat flux input within a rectangular enclosure. Their results showed that

the average Nusselt number increases with an increase of the Richardson number. Moraga and Lopez (2004) solved the equations of a laminar mixed convection developed in a parallelepipedic enclosure in which two vertical walls are maintained at uniform temperatures while the other four walls are adiabatic. An external air flow enters in the enclosure by a rectangular opening located near the top of one isothermal vertical wall and exits from another opening located near the bottom of the opposite isothermal vertical wall. Results show that the global Nusselt number can be deduced from a 3-D model for Re=500 and Ri<1, Re=30 and Ri<10, Re=80, for $Ri \geq 1$ and Re=50 for $Ri \geq 10$. A cell, observed near the vertical cold wall, causes differences between the global Nusselt numbers calculated from the 2-D and the 3-D models. For a predominantly natural convection flow (Ri=10 for $10 \leq Re \leq 250$), the velocity profiles must be deduced from a 3-D model. *Re*sults show that for Ri <1 and Re =500, Ri <10 and Re = 30, $Ri \geq 1$ and Re=80 and $Ri \geq 10$ and Re=50, the global Nusselt number must be determined from a 3-D model. Deng, Zhou, Mei and Shen (2004) studied the air flow and heat/contaminant transport structures in indoor air environement. Results highlight the effectiveness of using a visualisation with streamlines, isotherms, and iso-concentrations. The main objective of their study is an analysis of the two convection modes involved in a ventilated room by studying the effects of main factors, namely Grashof number, Reynolds number, buoyancy ratio, as well as the ventilation mode on transfers in this room. The air flow pattern depends on the relation between the natural and forced convection. In addition, their results show that the contaminant removal efficiencies depend on the importance of the two convection mechanisms. In order to study the energy stored in a cylindrical cavity in which a mixed convection is developed, Bouhjar and Harhad (2002) analysed numerically the effect of entrance cavity and the Richardson number on the flow. Results showed that the flow pattern for $Ri \leq 1$ is stable and the inertial forces are dominant, whereas for Ri>1, there is a transition phase in which the flow structure becomes unstable. The energy stored increases as the Ri number increases. Dehghan and Behnia (1996) reported an experimental study of mixed convection in open cavities formed by vertical strips with an aspect ratio equal to 0.4. It was shown, that the radiative heat transfer, for solar applications, is not negligible and that natural convection in open cavities in which walls are subjected to a uniform and constant heat flux density should be taken into account. Najam, Amahmid, Hasnaoui, and El Alami (2003) presented a numerical study on an unsteady mixed convection in a horizontal channel containing heating blocks periodically mounted on its lower wall while its upper wall is maintained at a uniform and constant temperature. The flow was assumed to be fully developed and periodic boundary conditions were used in the longitudinal direction of the channel. For large Reynolds number, the flow reduces considerably the heat transfer in the vicinity of the cold plate of the channel. Such a study was extended

6 years later by El Alami; Semma; Najam; and Boutarfam (2009). The governing equations were solved using a finite volume method and the SIMPLEC algorithm. Special emphasis was given to detail the effect of the Rayleigh number and blocks height on the heat transfer and the mass flow rate generated by natural convection. Djebali, El Ganaoui, Sammouda and Bennacer (2009) used the thermal lattice Boltzmann model to study natural convection in a heated rectangular cavity on a uniform grid. A general benchmark was carried out to account for the effect of different parameters in relatively wide ranges.

Carlson, Lin, and Chen (1997) studied heat exchanges for a 2D Cartesian geometry with adiabatic walls. Without obstacles the fluid flows through the cavity without an exchange of energy. A heating in the zone of recirculation exists but heat is not transferred to the principal flow. The obstacles increase the fluid velocities and consequently its temperature.

Islam et al. (2008) studied mixed convection inside an open cavity on the bottom of a channel. Three different cases were considered by applying uniform heat flux. The Galerkin weighted residual method of finite element formulation was used to discretize the governing equations. For mixed convection, the influential parameters are the Grashof number, Richardson number and Reynolds number. They studied velocity vectors, streamlines, isotherms, non-dimensional vertical velocities, maximum non-dimensional heated wall temperature and average Nusselt number of the heated wall. It was observed that the higher heat transfer occurs for opposing forced flow situation at low Richardson number. For higher Richardson number, a better thermal performance was achieved for the transverse flow case. Borjini, Cheikh, and Daguenet (1999) investigated numerically combined radiation and natural convection in a participating medium between two horizontal co-focal elliptical cylinders. The equations for steady, laminar, two-dimensional, natural convection flow were written by using an elliptic-cylinder coordinates system, and the stream function vorticity formulation. The finite volume radiation solution method and the control volume technique were used to discretize transfer equations. Numerical solutions were obtained for Rayleigh numbers in the range of 10^4 to 2.10^5 and the radiation-conduction parameter ranging from 0 to infinity. The special case corresponding to the convective flow within the annulus formed by an elliptical cylinder surrounding a flat plate was also considered. Effect of medium optical thickness, wall emissivity, scattering albedo, on fluid flow were studied.

The above literature review shows that most of these studies although encountered frequently in applications, focused on natural, forced convection or mixed convection. Combined mixed convection and radiation in open cavities has received little attention. So, in the present work, combined mixed convection and radiation in an open room model is investigated. This study is focused on the effect of radiation-

conduction parameter, the effect of optical thickness, and the effect of Boltzmann number on the thermofluid dynamics behaviour in an open enclosure model.

2 Mathematical Model

The schematic diagram of the square open enclosure physical model and the co-ordinates are shown in **Figure 1**. The height of the enclosure is L and the length W ($W = L$). The fluid (hot fumes, for example) enters the cavity through an inlet port of width $d_e = |y_2 - y_1|$ located at the left vertical wall. An exit port (towards the chimney) of width $d_s = |x_2 - x_1|$ is located on the middle of the top wall. The top and bottom walls are adiabatic and the other walls are maintained to different uniform temperatures.

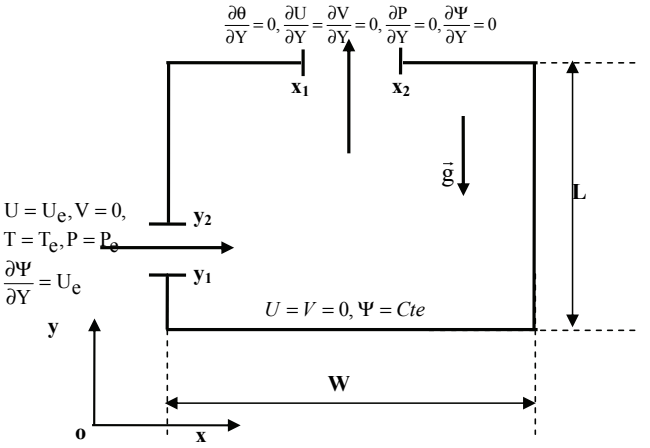

Figure 1: Open room physical model and coordinates system.

2.1 Hypothesis

Major assumptions adopted in this study are summarized below:

- No reactive phenomena are considered in this study,
- The flow is laminar and heat transfers are two-dimensional,
- The fluid is Newtonian and incompressible,
- The thermophysical properties of the fluids are constant
- The Boussinesq approximation is valid,

- The viscous dissipation is negligible,
- The walls are assumed to be gray and diffusely emitting and reflecting.

The governing equations in the Boussinesq approximation for laminar convection are given in dimensionless form as

$$\frac{\partial U}{\partial X}+\frac{\partial V}{\partial Y}=0 \tag{1}$$

$$\frac{\partial U}{\partial t}+\frac{\partial (UU)}{\partial X}+\frac{\partial (UV)}{\partial Y}=-\frac{\partial P}{\partial X}+\frac{1}{Re}\left(\frac{\partial^2 U}{\partial X^2}+\frac{\partial^2 U}{\partial Y^2}\right) \tag{2}$$

$$\frac{\partial V}{\partial t}+\frac{\partial (UV)}{\partial X}+\frac{\partial (VV)}{\partial Y}=-\frac{\partial P}{\partial Y}+\frac{1}{Re}\left(\frac{\partial^2 V}{\partial X^2}+\frac{\partial^2 V}{\partial Y^2}\right)+Ri\theta \tag{3}$$

$$\frac{\partial \theta}{\partial t}+\frac{\partial (U\theta)}{\partial X}+\frac{\partial (V\theta)}{\partial Y} = \frac{1}{Re\,\mathrm{Pr}}\left(\frac{\partial^2 \theta}{\partial X^2}+\frac{\partial^2 \theta}{\partial Y^2}\right)+\frac{R}{R-1}\frac{\tau}{Bo}\left\{G-4\left[\frac{\theta(R-1)+1}{R}\right]^4\right\} \tag{4}$$

$$\mu\frac{\partial I}{\partial X}+\xi\frac{\partial I}{\partial Y}=-\tau I+(1-\omega)\tau\theta^4+\frac{\omega\tau}{4\pi}\int_{\Omega'=4\pi} I\Phi(\vec{\Omega}',\vec{\Omega})d\Omega' \tag{5}$$

The stream function is calculated from;

$$U=\frac{\partial \Psi}{\partial Y},\quad V=-\frac{\partial \Psi}{\partial X} \tag{6}$$

So the equation (6) is written as:

$$\frac{\partial^2 \Psi}{\partial X^2}+\frac{\partial^2 \Psi}{\partial Y^2}=\frac{\partial U}{\partial Y}-\frac{\partial V}{\partial X} \tag{7}$$

With U and V are the velocity components in the X and Y directions respectively, Ψ is the dimensionless stream function. At solid boundaries Ψ is set equal to a constant, but at the inlet and the outlet the stream function is calculated as shown by equation (8) and (12.b) respectively. P is the pressure, and θ is the temperature. $\vec{\Omega}$ is the unit vector describing the radiation direction. $Re=U_e d_e/\nu$: Reynolds number, $\mathrm{Pr}=\nu/\alpha$: Prandtl number, and $Gr=g\beta\Delta T d_e^3/\nu^2$: Grashof number where ν is the kinematic viscosity, α the thermal diffusivity, β the thermal expansion coefficient of the fluid, and g is the gravitational acceleration. $Ri=Gr/Re^2$: the Richardson number, R: ratio between the inlet temperature and the ambient temperature; $R=$

T_h/T_C, R_C: radiation-conduction parameter defined as $R_C = d_e n^2 \tilde{\sigma} T_h^3/k$, Bo is the Boltzmann number $Bo = \rho C_p U_e/n^2\tilde{\sigma}T_h^3$ which gives the ratio between convection and radiation forces.

The left side of the equation (5) represents the gradient of the intensity in the direction of the radiation propagation, and the right hand side represents respectively, the attenuation of the intensity due to the absorption and the out scattering and the contribution to the directional intensity due to emission by the medium. The last term is the in-scattering of the radiative intensity. $\Phi(\vec{\Omega}', \vec{\Omega})$ is a probability density function; it determines the distribution of the scattered intensity. The lengths, velocities and pressure are dimensionlessed respectively by the inlet diameter d_e, the inlet velocity U_e, and by ρU_e^2, where ρ is the density of the fluid. $\theta = (T - T_C)/\Delta T$, with T_h and T_C are the temperatures of hot and cold wall, respectively. Time is dimensionlessed by U_e/d_e. The radiative intensity I is dimensionlessed by $n^2\tilde{\sigma}T_h^4$, the total intensity G by $n^2\tilde{\sigma}T_h^4$. To these equations we associated the following boundary conditions:

2.2 Boundary conditions

2.2.1 Left wall

- $X = 0$, $(y_1/d_e < Y < y_2/d_e)$ with (y_1=0.15 m and y_2=0.4 m)

$$U = \frac{\partial \Psi}{\partial Y} = 1, \quad V = -\frac{\partial \Psi}{\partial X} = 0, \theta = 1, \quad P = 1. \tag{8}$$

- $X = 0$; $(0 < Y < y_1/d_e)$ and $(y_2/d_e < Y < L/d_e)$

$$U = V = 0, \quad \Psi = Cte, \quad -\frac{\partial \theta}{\partial Y} + q_r R_c = 0 \tag{9}$$

2.2.2 Right wall

$X = L$, $0 < Y < L/d_e$

$$U = V = 0, \quad \Psi = Cte, \quad -\frac{\partial \theta}{\partial Y} + q_r R_c = 0 \tag{10}$$

2.2.3 Bottom wall

$Y = 0$, $0 < X < W/d_e$

$$U = V = 0, \quad \Psi = Cte, \quad -\frac{\partial \theta}{\partial X} + q_r R_c = 0 \tag{11}$$

2.2.4 Top wall

- $Y = H$, $(0 < X < x_1/d_e)$ and $(x_2/d_e < X < W/d_e)$ with x_1=0.4 m and x_2=0.6m

$$U = V = 0, \quad \Psi = Cte, \quad -\frac{\partial \theta}{\partial X} + q_r R_c = 0 \tag{12a}$$

- $Y = H$, $x_1/d_e < X < x_2/d_e$

$$\frac{\partial U}{\partial Y} = 0, \quad \frac{\partial V}{\partial Y} = 0, \frac{\partial \Psi}{\partial Y} = 0, \quad \frac{\partial P}{\partial Y} = 0 \tag{12b}$$

The radiation intensity is discretized as the following:

$$I^l = \varepsilon I_b + \frac{r}{\pi} \sum_{\vec{n}_1 . \vec{\Omega}' < 0} I^{l'} N_{cx}^{l'} \tag{13}$$

with $N_{cx}^l > 0$.
Where N_{cx}^l is the normalized direction cosine, and ε is the wall emissivity, r is the reflectivity. The divergence of the radiative heat flux, which is the source term in the energy equation, is given by:

$$div(\vec{q}_r) = \kappa_a (4\tilde{\sigma} T^4 - G) \tag{14}$$

Where G is the dimensionless total incident radiation written as follows:

$$G = \int_{\Omega'=4\pi} I(x, y, \vec{\Omega}) d\Omega \tag{15}$$

The radiative heat flux $\vec{q}_r$ is given by

$$\vec{q}_r = \int_{\Omega'=4\pi} \vec{\Omega} I(x, y, \vec{\Omega}) d\Omega \tag{16}$$

The bulk temperature is calculated as

$$\theta_b = \frac{\int_A \vec{V} \vec{n} \theta dA}{\int_A \vec{V} \vec{n} dA} \tag{17}$$

Where θ_b is the bulk temperature, $\vec{V}$ and $\vec{n}$ are the velocity vector and the inward normal vector, respectively. θ is the non dimensional temperature, A is the area perpendicular to the flow direction.

The local and average nusselt numbers are calculated by equations (18) and (19) respectively:

$$Nu_y = \frac{hy}{k} \tag{18a}$$

$$h(T_p - T_f) = -k \left.\frac{\partial T}{\partial y}\right|_{x=0} \tag{18b}$$

$$Nu_{mean} = \frac{1}{L}\int_0^L Nu(y)dy \tag{19}$$

3 Numerical Procedure

The equations (1-4) and the boundary conditions (8-12) are discretized by the finite-volume method. The discretized equations were solved by using the tri-diagonal matrix algorithm (TDMA) and an iterative process with a relaxation coefficient equal to 0.4 for velocity components and 0.8 for pressure and temperature. A two dimensional uniformly spaced staggered grid and a hybrid scheme was used for the convective terms, whereas a central difference scheme was used for the diffusive terms. The linkage between pressure and velocity variables is handled by the SIMPLE algorithm developed by Pantakar (1980).

The iterative procedure is repeated when the following test is verified:

$$\max\left(\left|\Phi^n - \Phi^{n-1}\right| / \Phi^n\right) \leq \varepsilon \tag{20}$$

where n is the number of iteration, ε the precision criteria equal to 10^{-5} for the radiative intensity and 10^{-8} for the source term of the pressure equation.

4 Resolution of the Radiative Heat Transfer Equation

The equation (5) associated with the boundary conditions (13) are solved using the finite volume method (FVM) for radiation, Raithby and Chui (1990), Chai, Lee, and Patankar (1994). The total solid angle is subdivided in an arbitrary number of control angles. The angular space is subdivided in a certain number of control volumes. The final discretization equation for a general control volume and control angle can be written as

$$a_P^l I_P^l = a_w^l I_W^l + a_e^l I_E^l + a_s^l I_S^l + a_n^l I_N^l + b^l \tag{21}$$

where

$$a_i^l = \max\left[-\Delta A_i D_{ci}^l, 0\right] \quad i = w, e, s, \text{ and } n \tag{22a}$$

$$a_P^l = \sum_i^{nb} \max\left[\Delta A_i D_{ci}^l, 0\right] + \left(\beta_m^l\right)_P \Delta v \Delta\Omega^l \quad nb = \text{all neighbor} \tag{22b}$$

$$b^l = \left(S_m^l\right)_P \Delta V \Delta\Omega^l \tag{22c}$$

$$D_{ci}^l = \int_{\Delta\Omega^l} (\hat{s} \bullet \hat{n}_i)\, d\Omega \tag{22d}$$

$$\Delta\Omega^l = \int_{\phi^{l-}}^{\phi^{l+}} \int_{\theta^{l-}}^{\theta^{l+}} \sin\theta d\theta d\phi \tag{22e}$$

$$\beta_m^l = \kappa_a + \sigma - \frac{\sigma}{4\pi} \bar{\Phi}^{ll} \Delta\Omega^l \tag{22f}$$

$$S_m^l = \kappa_a I_b + \frac{\sigma}{4\pi} \sum_{l'=1, l' \neq l}^{L} \bar{\Phi}^{l'l} \Delta\Omega^{l'} I^{l'} \tag{22g}$$

$$\hat{s} = (\sin\theta\cos\phi)\,\hat{e}_x + (\sin\theta\sin\phi)\,\hat{e}_y + (\cos\theta)\,\hat{e}_z \tag{22h}$$

$$\bar{\Phi}^{l'l} = \frac{\int_{\Delta\Omega^l} \int_{\Delta\Omega^{l'}} \Phi\left(\hat{s}', \hat{s}\right) d\Omega' d\Omega}{\Delta\Omega^l \Delta\Omega^{l'}} \tag{22i}$$

The step scheme is used in the present work, although other spatial differencing schemes (Positive, Hybrid, and CLAM) can also be used with the proposed procedure.

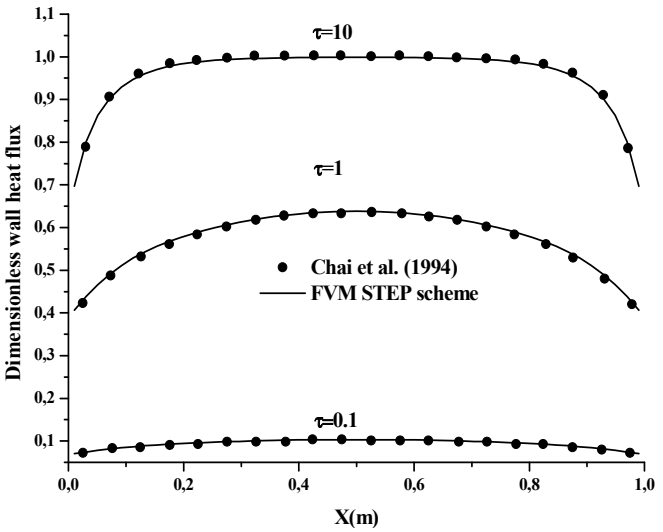

Figure 2: Dimensionless bottom wall heat flux.

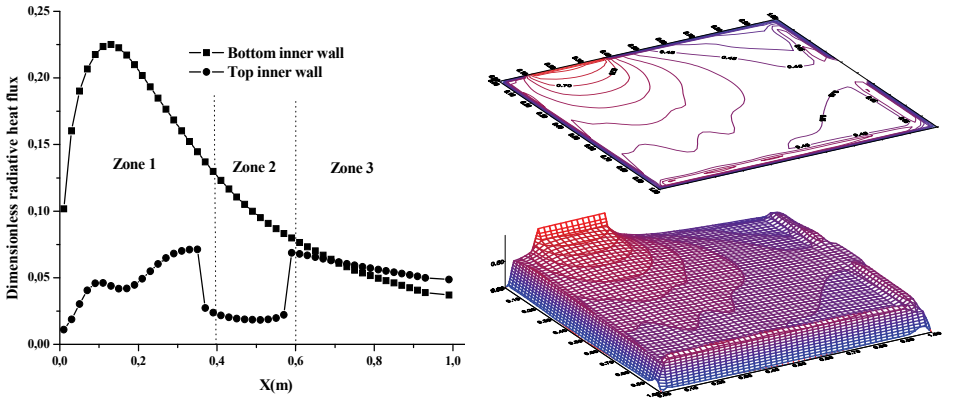

Figure 3: (a) Dimensionless bottom inner wall and top inner wall radiative heat flux; (b) Temperature distribution inside the studied configuration (pure radiation).

5 Validation

5.1 Radiative transfer

In order to validate our radiative numerical method, we propose to compare our results with the most closely related numerical solutions. **Figure 2** shows the dimensionless bottom wall heat flux obtained with our radiative numerical code applied to a 2D enclosure filled with a gray, absorbing, emitting, and non-scattering semi-transparent medium and the results deduced from the solution of Chai, Lee, and Patankar (1994). Three optical thicknesses τ=0.1, 1 and 10 are considered. The used spatial and angular grid meshes are respectively $(N_x \times N_y) = (21 \times 21)$ and $(N_\theta \times N_\varphi) = (4 \times 24)$. The dimensionless heat flux is defined as the heat flux divided by the gas blackbody emissive power. We notice that the FVM (STEP scheme) results are in good agreement with the exact solution Chai, Lee, and Patankar (1994). **Figure 3.a** shows, for pure radiation, the dimensionless bottom inner wall radiative heat flux and top inner wall radiative heat flux and the isotherm inside a cavity with inlet and outlet ports. We observe that at the bottom wall, the dimensionless radiative heat flux is important at x=0.15 whereas between x=0 and x=0.1 the radiative heat flux is minimal. Between x=0.2 and x=1 the radiative heat flux is decreasing versus x coordinate. The dimensionless top inner wall radiative heat flux is plotted also on **Figure 3.a**. It can be divided into three zones. The zone 1, located between x=0 and x=0.4, is influenced by the heating coming from the inlet. Zone 2 is located between x=0.4 and x=0.6. This is the cavity outlet where we can see that the radiative heat flux is approximately null. The third zone is situated between x=0.6

and x=1 where we notice that the radiative heat flux is also decreasing versus x coordinate. **Figure 3.b** gives the temperature pattern in the medium obtained from a radiation code. One can see that in the vicinity of the inlet the temperature is higher whereas the temperature decreases far from the inlet. Even the edges of the cavity are heated which can not be seen in a pure conduction problem.

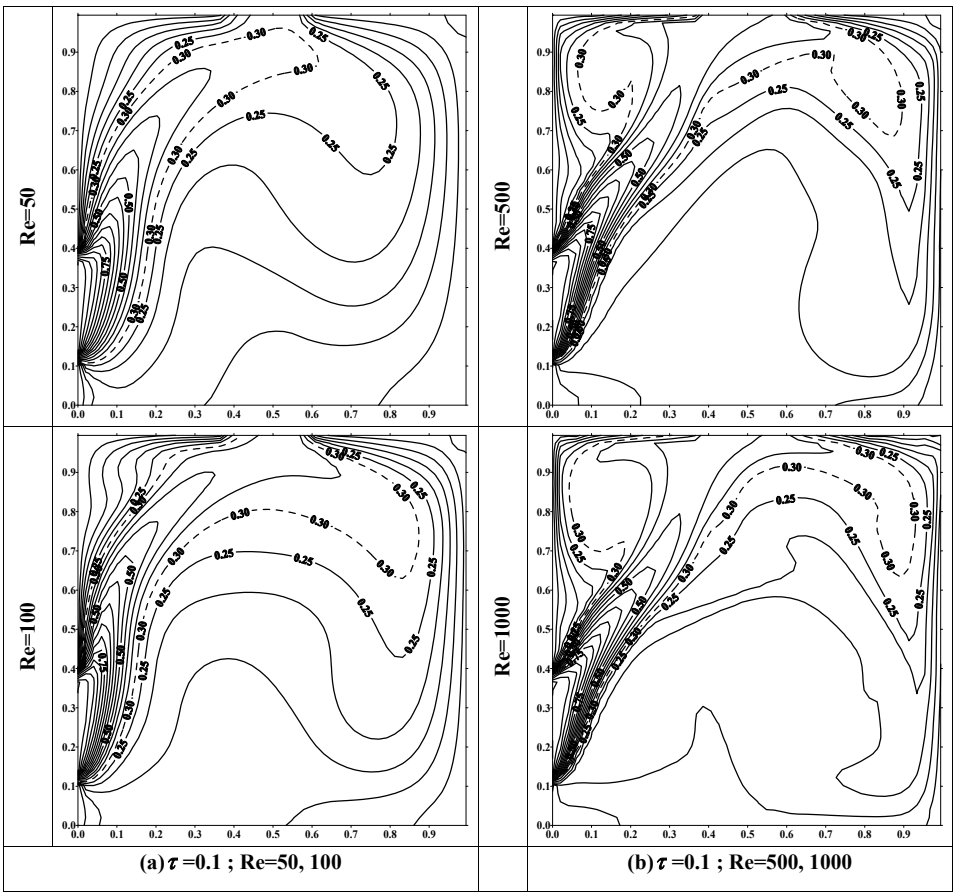

Figure 4: Isotherm distributions τ=0.1. Effect of Reynolds number; (a) *Re*=50; *Re*=100; (b) *Re*= 500; *Re*=1000.

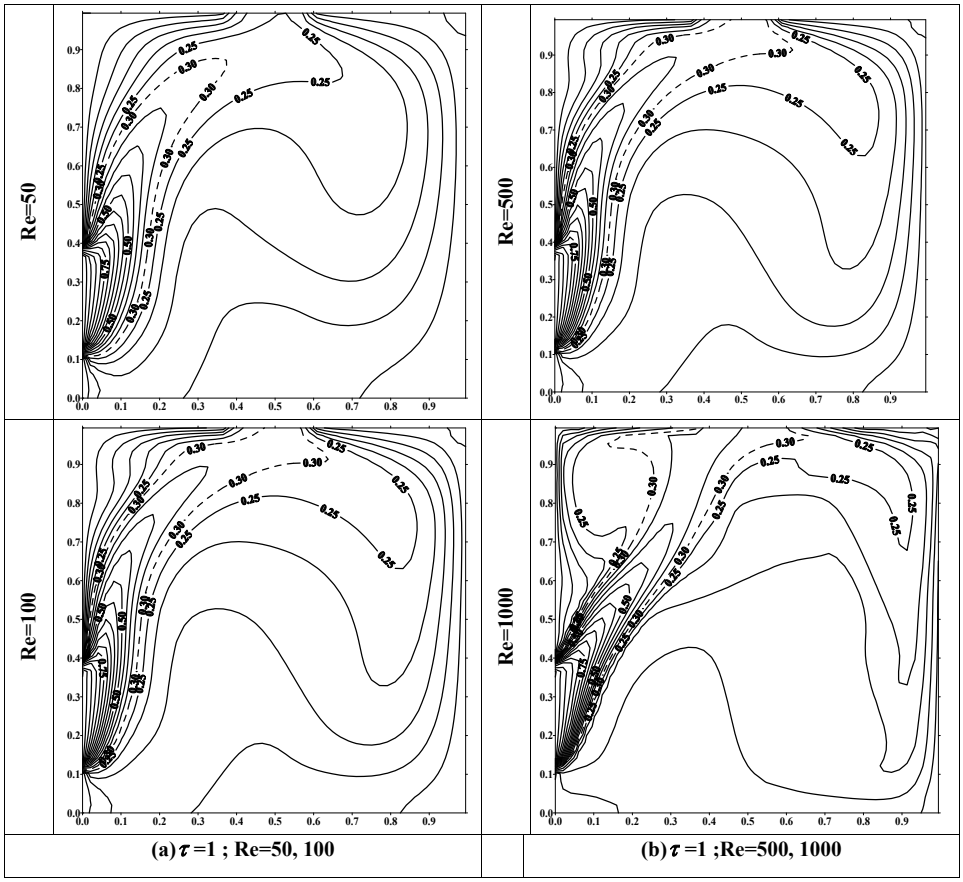

Figure 5: Isotherm distributions τ=1. Effect of Reynolds number; (a) *Re*=50; *Re*=100; (b) *Re*= 500; *Re*=1000.

6 Combined Mixed Convection and Radiation

6.1 Effect of optical thickness

Figures 4, 5, 6 show isotherms distribution for $\varepsilon = 1$,$\omega = 0$, *Bo*=1, *Rc*=1, R=2, *Re*=50, 100, 500, and 1000, and *Ri*=0.01, and for different values of the optical thickness ranging from thin to thick optical mediums τ = 0.1, 1 and 10. As illustrated in **Figure 4** the participation of the medium for thin optical thickness ($\tau < 1$) to the radiative transfers is small and the energy is easily transferred from the hot region (inlet) to the other cold ones. For large optical thickness ($\tau = 10$), the isotherms are clustered near the inlet, the radiative heat transfer at the right-

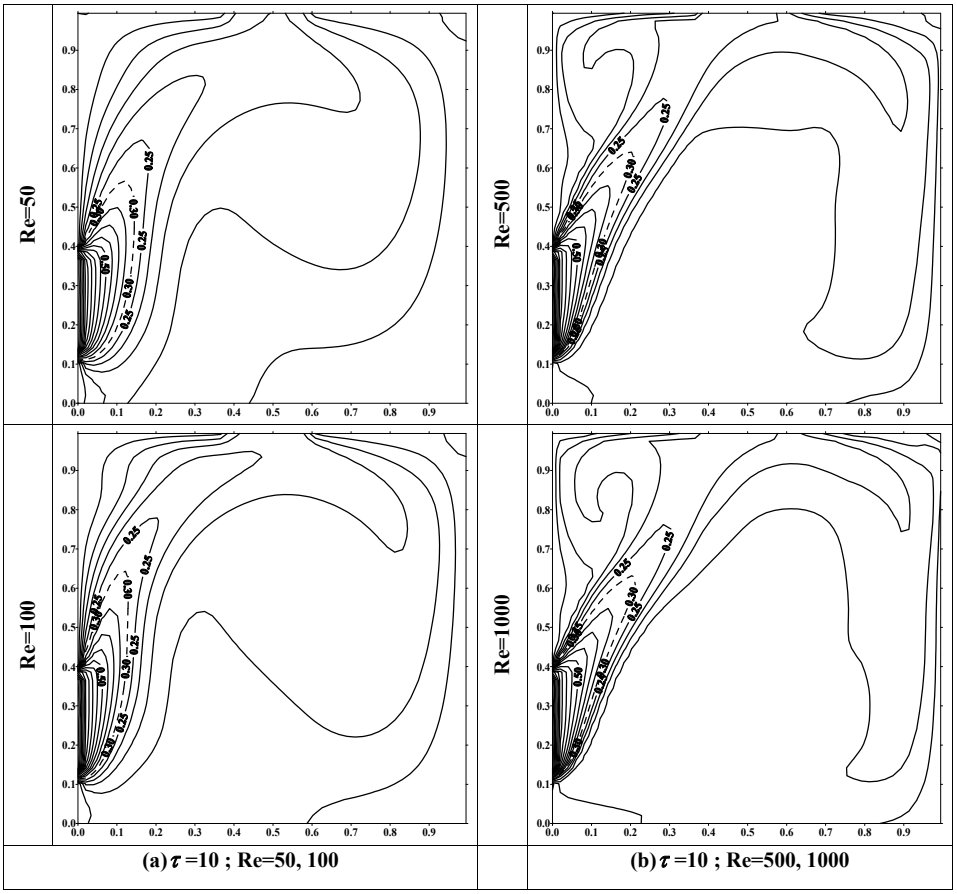

Figure 6: Isotherm distributions τ=10. Effect of Reynolds number; (a) *Re*=50; *Re*=100; (b) *Re*= 500; *Re*=1000.

hand wall becomes small enough to be neglected; this can be seen from isotherm 0.3(**Figure 6**). In fact for $\tau = 0.1$, the maximum distance for the isotherm 0.3 in the entry direction is equal to *x*=0.6, and the maximum distance in the outlet direction is *y*=0.95. The bulk temperature at the right-hand wall is also getting higher. The participating medium gives lower values of the bulk temperature than the non-participating one because the radiative heat fluxes at the cold wall decrease as the optical thickness increases (**Figure 7**). The average Nusselt number at the wall containing the entry increases as the optical thickness increases (**Figure 8**).

The temperature evolutions plotted in **Figures 9** and **10** versus the *x* and *y* directions respectively for different optical thicknesses show that the temperature in-

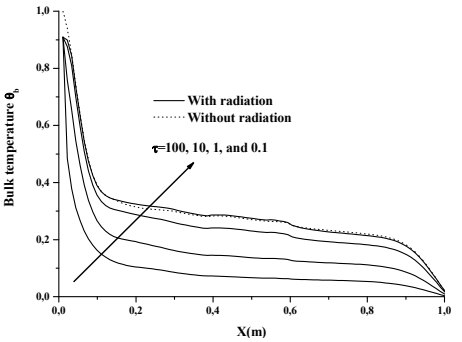

Figure 7: Effect of the optical thickness on the bulk temperature.

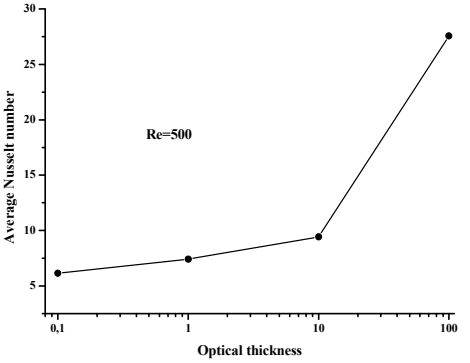

Figure 8: Effect of the optical thickness on the average Nusselt number.

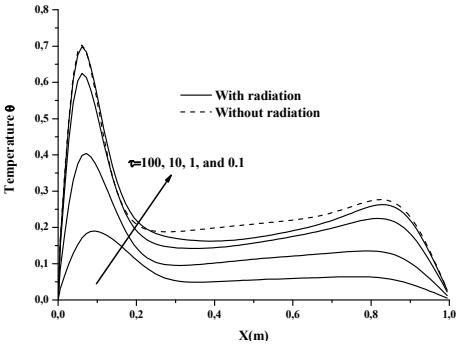

Figure 9: Effect of the optical thickness on the temperature.

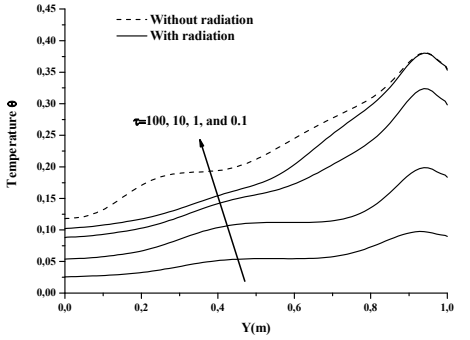

Figure 10: Effect of the optical thickness on the temperature evolution versus the Y direction.

creases when the optical thickness decreases. In fact, when the optical thickness of the medium increases it becomes more participant to the radiative exchanges. Therefore radiative intensity can't easily move to the other adiabatic walls of the cavity because it is absorbed or scattered by the medium; this explains that the inertia of the medium increases with increasing optical thickness and consequently the medium temperature increases.

6.2 Effect of Radiation-Conduction Parameter

In this section, the calculations have been carried out to investigate the effects of radiation-conduction parameter which characterizes the relative importance of radiation with respect to conduction. The effect of radiation is getting strong as the *Rc*

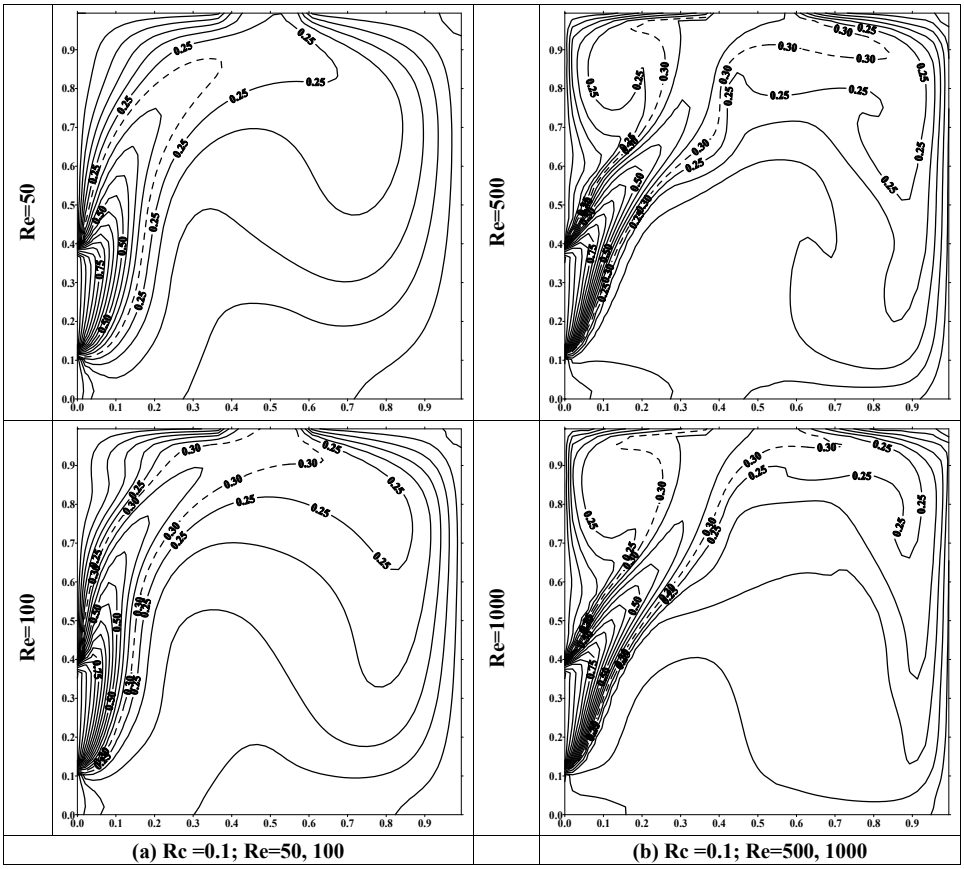

Figure 11: Isotherm distributions *Rc*=0.1. Effect of Reynolds number; (a) *Re*=50; *Re*=100; (b) *Re*= 500; *Re*=1000.

increases. Physically, an increase in *Rc* induces an increase of the radiation effect toward conduction. Mathematically, in the equations giving the boundary conditions, an increase in *Rc* means that the radiative heat flux on the walls becomes more significant than the conductive heat flux. Accordingly, the medium temperature in the enclosure is shown to be higher for high *Rc* numbers. The results are obtained for $\tau = 1$, $\varepsilon = 1$, $\omega = 0$, *R*=2, *Bo*=1, *Re*=1000, and *Ri*=0.001. **Figures 11**, **12** and **13** show temperature profile for *Rc*=0.1, 1 and 100. When *Rc*<1, the isotherms are very tight close to the cold walls (**Figure 11**). As *Rc* increases, a steeper temperature gradient is formed at both y=0 and y=L walls and the temperature medium far from the inlet (hot surface) increases. In fact, the radiative energy emitted from the hot wall can penetrate more deeply into the medium and is therein

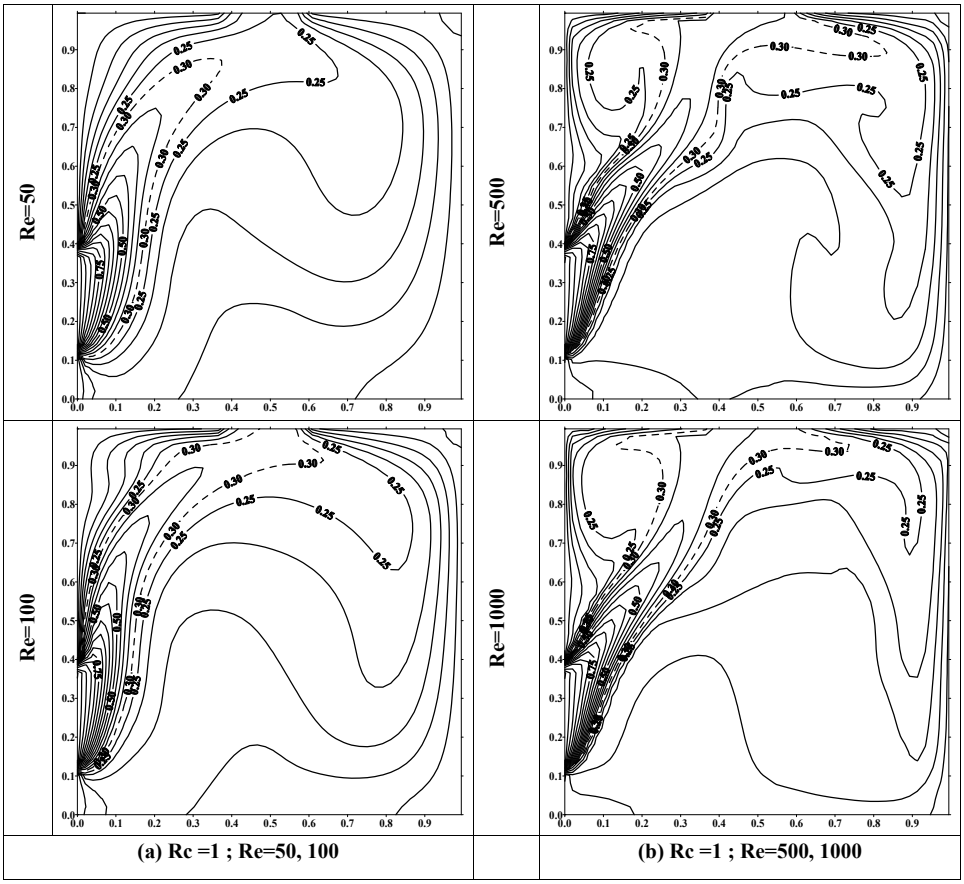

Figure 12: Isotherm distributions *Rc*=1. Effect of Reynolds number; (a) *Re*=50; *Re*=100; (b) *Re*= 500; *Re*=1000.

transformed into thermal energy. These results are in agreement with those of Kim and Baek (1991). One can note the temperature increasing at the right top of the enclosure when *Rc* rises (**Figures 12, 13**). The *Rc* number does not occur explicitly in the momentum equation; its effect on the velocity field is indirect. Hence the velocity field is weakly dependent on *Rc*. Therefore, the results are not shown here (streamlines). It is seen that streamlines are not apparently influenced by *Rc* in the entrance region, since the forced convection is predominant knowing that the velocity gradient is small in this region. This may be explained by the fact that the temperature field is flattened with the presence of radiation causing a reduction of buoyancy effect, which in turns leads to the reduction of velocity values at the

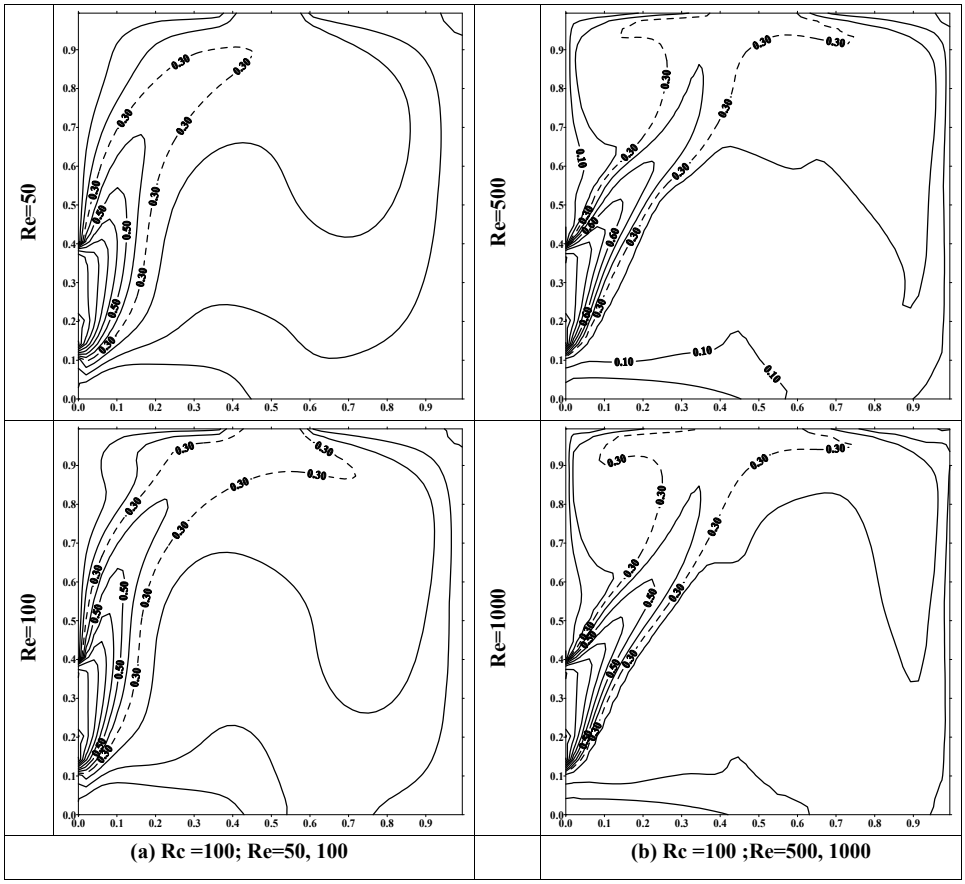

Figure 13: Isotherm distributions *Rc*=100. Effect of Reynolds number; (a) *Re*=50; *Re*=100; (b) *Re*= 500; *Re*=1000.

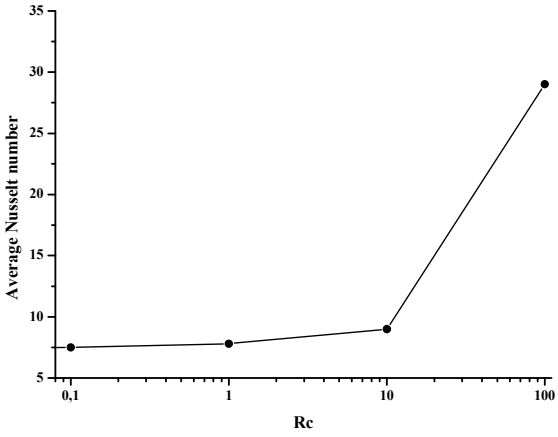

Figure 14: Average Nusselt number versus the radiation conduction parameter

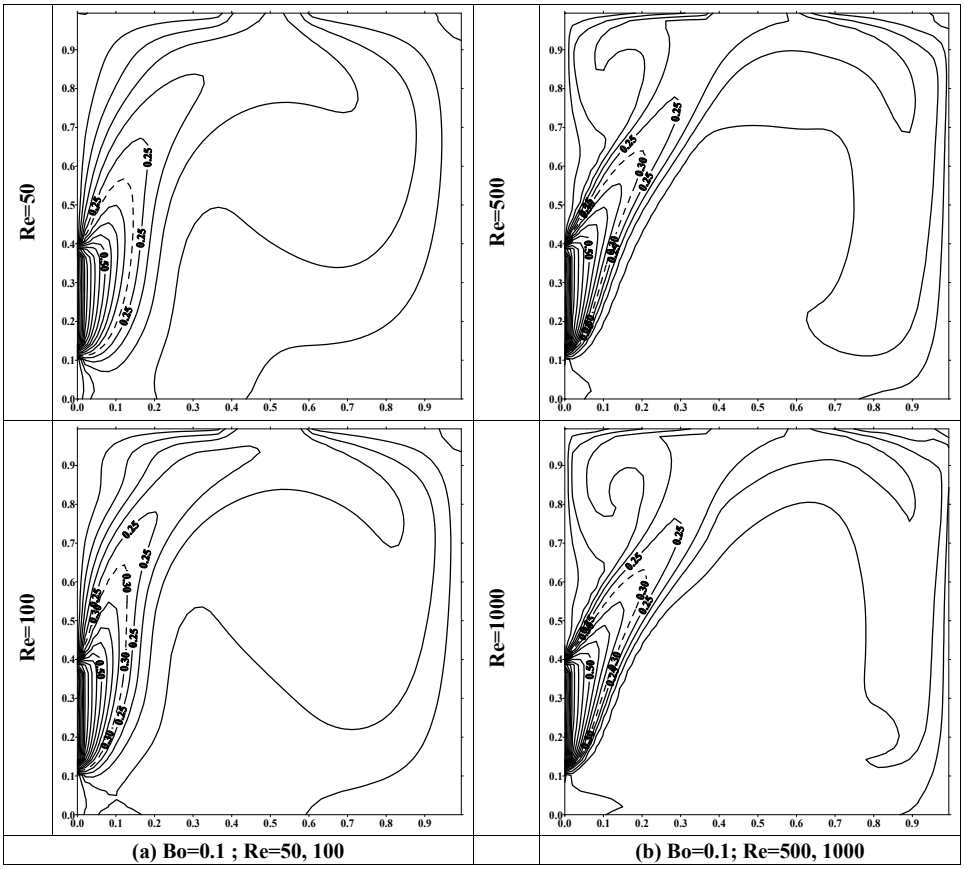

Figure 15: Isotherm distributions. *Bo*=0.1. Effect of Reynolds number; (a) *Re*=50; *Re*=100; (b) *Re*= 500; *Re*=1000.

upstream. **Figure 14** gives the evolution of the average Nusselt number versus the *Rc* number; we found that the average Nusselt number increases with an increasing of the *Rc* number. In fact, when the *Rc* number increases the transfers by radiation becomes more important than those by conduction on the walls, therefore the heat rate transferred to the medium increases which explains the augmentation of the Nusselt number.

6.3 Effect of Boltzmann Number

The Boltzmann number characterizes the relative importance of convection transfer with respect to radiation transfer. The effect of convection transfer is getting strong as Bo increases. Physically, a decrease in Bo results in an increase in the source

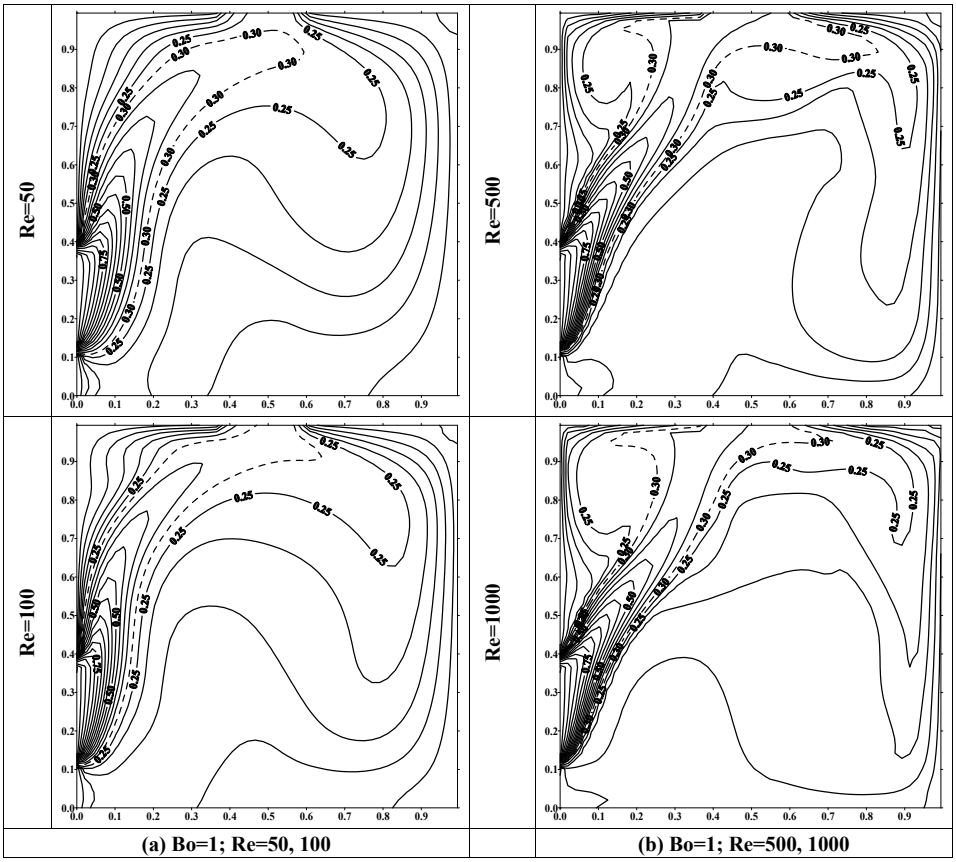

Figure 16: Isotherm distributions. *Bo*=1. Effect of Reynolds number; (a) *Re*=50; *Re*=100; (b) *Re*= 500; *Re*=1000.

term in the energy equation (4); so that, more radiant energy is absorbed and transformed into thermal energy. **Figures 15, 16** and **17** show isotherm distributions for $\tau = 1$, $\varepsilon = 1$, $\omega = 0$, R=2, *Rc*=1, *Re*=50, 100, 500, 1000, and *Ri*=0.01, and for different values of the Boltzmann number ranging from convection dominating mode to radiation dominating mode, *Bo*=0.1, 1, and 100. As shown in **Figure 15**, for small Bo numbers, the temperature distribution is clustered near the inlet of the cavity and directed toward the outlet. Whereas, if *Bo* increases the radiation mode becomes more important and more energy is transferred by convection to the other cold walls. For *Re*=500, if *Bo*=0.01, the isotherm 0.3 (dashed lines) is clustered to the inlet, then for *Bo*=0.1 the isotherm 0.3 attains the location (x=0.2, y=0.63) and for *Bo*=100, the isotherm attains the right wall in the x-direction and the top wall in

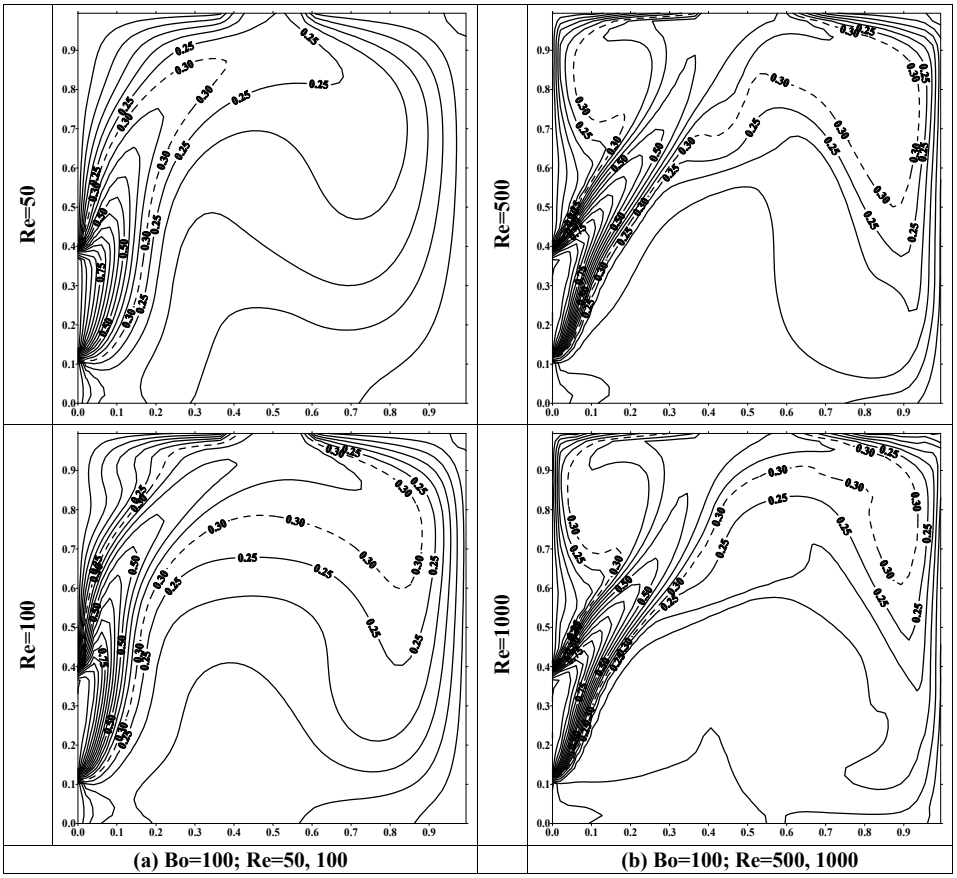

Figure 17: Isotherm distributions. *Bo*=100. Effect of Reynolds number; (a) *Re*=50; *Re*=100; (b) *Re*= 500; *Re*=1000.

the y-direction. The bulk temperature at the right-hand wall is also getting higher (**Figure 18**). Consequently, the average Nusselt number is shown to increase as the Boltzmann number increases (**Figure 19**).

7 Conclusion

A numerical study about combined thermal radiation and laminar mixed convection for a gray fluid inside an open square cavity with inlet and outlet ports is investigated. The non dimensional transfer equations and the radiative transfer equation are solved by the finite-volume-method. Results are presented for a wide range of Reynolds number, Richardson number, Boltzmann number, conduction radiation

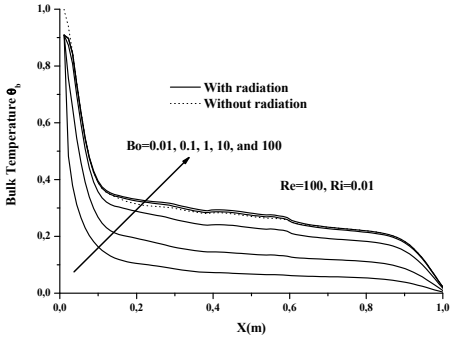

Figure 18: Effect of the Boltzmann number on the bulk temperature profile.

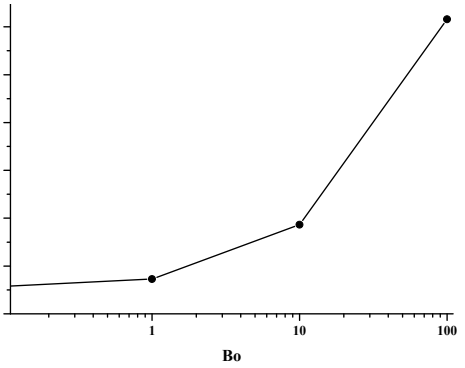

Figure 19: Evolution of the average Nusselt number versus the Boltzmann number.

number and the optical thickness. The effects are emphasized on radiative transfer for a gray fluid development of streamlines and temperature fields. In the presence of radiation, the thermal development develops at a more rapid rate relative to that without radiation. The average Nusselt number is increased by increasing optical thickness of the gray medium, and the radiation to conduction parameter *Rc*. The average Nusselt number decreases as the Boltzmann number increases. The bulk temperature increases as the Boltzmann number increases and decreases as the optical thickness increases. Finally, this work can be improved by taking into account the non-gray gas behaviour and extending the code to a 3D model.

References

Accary G.; Meradji S.; Morvan D.; Fougere D. (2008): Towards a Numerical Benchmark for 3D Low Mach Number Mixed Flows in a Rectangular Channel Heated from Below *FDMP: Fluid Dynamics & Materials Processing*, Vol. 4, No. 4, pp. 263-270.

Ben-Arous A. M.; Busedram A. A. (2008): Mixed Convection in Horizontal Internally Finned Semicircular Ducts *FDMP: Fluid Dynamics & Materials Processing*, Vol. 4, No. 4, pp. 255-262.

Borjini M. N.; Cheikh M.; Daguenet M. (1999): Numerical Analysis Of The Effect Of Radiation On Laminar Steady Natural Convection In A Two-Dimensional Participating Medium Between Two Horizontal Co-Focal Elliptical Cylinders, *Numerical Heat Transfer A*, Vol. 35, pp. 467-94.

Bouhjar A.; Harhad A. (2002): Numerical Analysis Of Transient Mixed Con-

vection Flow In Storage Tank: Influence of Fluid Properties and Aspect Ratios on Stratification, *Renewable Energy*, Vol. 25, pp. 555-67.

Carlson K. D.; W. L. Lin; Chen C.-J. (1997): Pressure Boundary Conditions Of An Incompressible Flows With Conjugate Heat Transfer On Non Staggered Grids, Part I: Applications, *Numerical heat transfer*, Part A, Vol. 32, pp.481-01.

Chai, J. C.; Lee, H. S.; Patankar, S. V. (1994): Finite-Volume Method For Radiation Heat Transfer, *Journal Of Thermophysics And Heat Transfer*, Vol. 8, No. 3, pp. 419-25.

Dehghan A. A; Behnia M. (1996): Combined Natural Convection-Conduction And Radiation Heat Transfer In A Discretely Heated Open Cavity, *J. Heat Transfer*, vol. 118, pp. 56–64.

Deng Q. H.; Zhou J. M.; Mei C.; Shen Y. M. (2004): Fluid, Heat and Contaminant Transport Structures Of Laminar Double-Diffusive Mixed Convection In A Two Dimensional Ventilated Enclosure, *International Journal of Heat and Mass Transfer*, Vol. 47, pp. 5257-69.

Djebali R., El Ganaoui M., Sammouda H. and Bennacerm R. (2009): Some Benchmarks of a Side Wall Heated Cavity Using Lattice Boltzmann Approach, *FDMP: Fluid Dynamics & Materials Processing* Vol. 5, No. 3, 261.

El Alami M.; Semma E. A.; Najam M.; Boutarfam R. (2009): Numerical Study of Convective Heat Transfer in a Horizontal Channel, *FDMP: Fluid Dynamics & Materials Processing*, Vol. 5, No. 1, pp. 23-36.

Islam Md. T.; Saha S.; Hasan Mamun Md. A.; Ali M. (2008): Two Dimensional Numerical Simulation of Mixed Convection in a Rectangular Open Enclosure *FDMP: Fluid Dynamics & Materials Processing*, Vol. 4, No. 2, pp. 125-138.

Kim T.Y; Baek S. W. (1991): Analysis Of Combined Conductive And Radiative Heat Transfer In A Two-Dimensional Rectangular Enclosure Using The Discrete Ordinates Method, *International Journal of Heat and Mass Transfer*, Vol. 86, pp. 2265-73.

Moukalled F.; Darwish M. (1997): A New Family Of Stream Line-Based Very High Resolution Schemes, *Numerical Heat Transfer B*, Vol. 31, pp. 91-110.

Najam M.; Amahmid A.; Hasnaoui M.; El Alami M. (2003): Unsteady Mixed Convection in a Horizontal Channel with Rectangular Blocks Periodically Distributed on Its Lower Wall, *International Journal of Heat and Fluid flow*, Vol. 24, pp. 726-35.

Nelson O. Moraga; Sergio E. Lopez (2004): Numerical Simulation Of Three Dimensional Mixed Convection In An Air Cooled Cavity, *Numerical Heat Transfer*, Part A, vol. 45, pp. 811–24.

Omri A.; Nasrallah S. B. (1999): Control Volume Finite Element Numerical Simulation Of Mixed Convection In An Air Cooled Cavity, *Numerical Heat Transfer A*, Vol. 36, pp. 615-37.

Papanicolaou E.; Jaluria Y. (1990): Mixed Convection From An Isolated Heat Source In A Rectangular Enclosure, *Numerical Heat Transfer*, Part A, vol. 18, pp. 427–61.

Patankar S. V. (1980): *Numerical Heat Transfer And Fluid Flow*, Mc Graw Hill, New York.

Raithby G. B.; Chui E. H. (1990): A Finite Volume Method For Predicting A Radiant Heat Transfer In Enclosures With Participating Media, *J. Heat Transfer* vol. 112, pp. 415-23.